MECHANICAL CHARACTERIZATION OF SILICON CARBIDE COMPOSITES FOR HFIR-18J EXPERIMENT IN UNIRRADIATED CONDITION — Y. Katoh, K. Ozawa, L.L. Snead (Oak Ridge National Laboratory), Y.B. Choi (Hiroshima University), T. Hinoki (Kyoto University), and A. Hasegawa (Tohoku University)

OBJECTIVE

This work has as an objective of determining the mechanical properties of the silicon carbide composite materials produced for the purpose of evaluating high temperature irradiation performance in the HFIR-18J experiment.

SUMMARY

A suite of silicon carbide ceramics and composite materials were prepared in various specimen types for the purpose of evaluating irradiation performance at high to very high temperatures in the HFIR RB-18J experiment. Detailed information of the materials prepared is provided. Properties including tensile strength, dynamic elastic modulus, interlaminar shear strength, and trans-thickness tensile strength were determined in an unirradiated condition.

PROGRESS AND STATUS

Introduction

Silicon carbide (SiC) ceramics and continuous fiber composites are promising commercial materials for fusion applications due to the exceptional radiation stability, high temperature performance, and low activation properties inherent to SiC. An extensive neutron irradiation campaign HFIR-18J was carried out in US-Department of Energy/Japan-MEXT (Ministry of Education, Culture, Sports, Science and Technology) fusion blanket/materials collaboration program for the purposes of 1) gaining a fundamental understanding of irradiation effects in SiC composites and their constituents in aggressive, fusion-relevant conditions, 2) determining the effects of neutron irradiation on various properties of new generation materials, 3) advancing constitutive modeling of irradiation effects in composites, and 4) determining irradiated engineering properties in support of blanket systems research and development.

In the HFIR-18J experiment, composite materials were fabricated with three different near-stoichiometric SiC fibers and/or high thermal conductivity graphite fibers, thin, ultra-thin, or multilayer interphases, and the SiC matrix made through chemically vapor-infiltration (CVI) or transient eutectic-phase (NITE; nano-infiltration and transient eutectic-phase) processes are being evaluated for mechanical and transport properties following irradiation up to ~7 dpa at temperatures nominally in an 800-1300ºC range. Properties such as axial tensile strength, dynamic elastic modulus, interlaminar shear strength, and trans-thickness tensile strength in an unirradiated condition are given in this report, in addition to the detailed information of materials preparation.

Experimental Procedure

Materials

Materials tested in the HFIR-18J experiment are listed in Table 1. The monolithic SiC ceramics included in the experimental matrix are Rohm & Haas chemically vapor-deposited (CVD) SiC, Coorstek CVD SiC, Hoya single crystal 3C-SiC, and a liquid phase-sintered SiC which represents the matrix material of the NITE composites. Coorstek CVD SiC is of similar chemical purity with the Rohm & Haas but have smaller grain sizes. The high electrical resistivity grade CVD SiC was included to examine the post irradiation electrical properties.

Table 1 – Details of SiC and SiC/SiC materials

Material	Abbreviation	Code	Identifier Prefix	Description (for composites, fiber / interphase / matrix)
CVD SiC R&H	CVD-SiC	CD1	R	Rohm & Haas Co. CVD-SiC, Standard resistivity grade SC-001, Lot# 9130
CVD SiC Coors	CVD-Coors	CD2	C	Coorstek Pure-SiC CVD-SiC, Standard grade, Lot# 549220-1
Single-Crystal 3C-SiC	SC-SiC	SXS	n/a	Hoya single crystal 3C-SiC, Lot# SBB12AH, N-doped 9.53E+18 cm^{-3}
NITE Matrix SiC	LPS-SiC	LPS	L	Liquid phase-sintered SiC for matrix of NITE SiC/SiC, Lot# KS05
HR-Grade CVD SiC R&H	HR-SiC	CD3	D	Rohm & Haas Co, CVD-SiC, High-resistivity grade SC-003, Lot# 9191
TySA CVI Reference	TySA-CVI-Ref	TRF	T	Tyranno-SA3 7.5 micron (SA3-S1I16PX), 2D Plain Weave (PSA-S17I16PX), 17x17 tpi / PyC(150nm) / CVI-SiC
TySA CVI Thin Interphase	TySA-CVI-TI	TTI	X	Tyranno™-SA Grade-3 7.5 micron (SA3-S1I16PX), 2D Plain Weave (PSA-S17I16PX), 17x17 tpi / PyC(50nm) / CVI-SiC
TySA CVI Thick Fiber	TySA-CVI-TF	TTF	F	Tyranno™-SA Grade-3 10 micron (SA3-S1F08PX), 2D Plain Weave (PSA-S17F08PX), 17x17 tpi / PyC(150nm) / CVI-SiC
Nicalon-S CVI Reference	HNLS-CVI-Ref	SRF	A	Hi-Nicalon™ Type-S 900denier (#383213), 2D Plain Weave (HNS9P2424), 24.25x25 tpi / PyC(150nm) / CVI-SiC
Nicalon-S CVI Thin Interphase	HNLS-CVI-TI	STI	E	Hi-Nicalon™ Type-S 900denier (#383213), 2D Plain Weave (HNS9P2424), 24.25x25 tpi / PyC(50nm) / CVI-SiC
Nicalon-S CVI ML Interphase	HNLS-CVI-ML	SML	M	Hi-Nicalon-S 2D-PW(0/90) / (PyC/SiC) multilayer interphase / CVI-SiC
SiC/C Hybrid Fabric CVI	Hybrid-CVI	HFC	H	Tyranno-SA3 7.5 micron (SA3-S1I16PX) / P-120S Graphite Fiber, Orthogonal 3D Weave / PyC(150nm) / CVI-SiC
TySA NITE Composite PG3	TySA-NITE	NTE	N	Tyranno-SA3 UD-XP / PyC / NITE-SiC PG3, Lot# 0408
TySA NITE Composite LG06	TySA-NITE-LG	NTL	K	Tyranno-SA3 UD / PyC / NITE-SiC Lab-Grade #LG06, Lot# LG06
TEM in Graphite Tube	SiC-TEM-Tube	TEM	P	Coated TEM discs for He-injection in SiC tube
Fiber in Graphite Tube	SiC-Fiber-Tube	FBR	P	SiC fiber bundle in SiC tube
Ceramics in TZM Tube	TZM-Tube	TZM	P	Lithium oxide ceramics and diffusion pairs in sealed TZM packet
NITE Joint	SiC-Joint	JNT	J	CVD-SiC joint by NITE, provided by Kyoto University
GE Nicalon-S ICVI	HNLS-CVI-GE	GES	S	GE Power Systems Hi-Nicalon-S 2D-SW / PyC / ICVI-SiC, Provided by PNNL
JAERI 3D Nicalon-S ICVI	HNLS-CVI-3D	JHC	YR	Hi-Nicalon-S 3D / PyC / ICVI-SiC, provided by PNNL
JAERI 3D TySA ICVI	TySA-CVI-3D	JTC	YR	Tyranno-SA 3D / PyC / ICVI-SiC, provided by PNNL
JAERI 3D TySA ICVI-PIP	TySA-CVI-PIP	JTP	YR	Tyranno-SA 3D / PyC / (ICVI+PIP)-SiC, provided by PNNL

The composite materials were prepared by CVI or NITE matrix densification process. For the two dimensional (2D) CVI composites, either Tyranno™-SA3 7.5um fibers, Tyranno™-SA3 10um fibers, or Hi-Nicalon™ Type-S fibers were used as the reinforcement, either in plain-weave or satin-weave architecture with the 0/90º stacking sequence. An orthogonal three-dimensional (3D) CVI composite was

also prepared incorporating Tyranno™-SA3 fibers in the in-plane directions and a high thermal conductivity pitch-based graphite fiber P-120S in the through-thickness direction. Limited data of the mechanical and thermophysical properties of these composites were previously determined and published. [5] The NITE composites were prepared using Tyranno™-SA3 fibers in the uni-directional (UD) or UD cross-ply architecture and relatively thick pyrocarbon interphase. [3]

Included in the graphite TEM tubes were transmission electron microscopy disc samples of the standard resistivity grade Rohm & Haas CVD SiC and Hoya single crystal 3C-SiC. Some of the samples were coated with NiAl for the purpose of examining the effect of in-situ helium injection on microstructural development. In the fiber tubes, Tyranno™-SA3 and Hi-Nicalon™ Type-S bare fibers were included.

The CVD SiC joint samples with the NITE joining were provided by Kyoto University. Details of the NITE joint is provided elsewhere.[1] The GE Power Systems (currently GE Energy) isothermal CVI composite was provided by the Pacific Northwest National Laboratory (PNNL). The three isothermal CVI and CVI+polymer impregnation and pyrolysis (PIP) hybrid matrix composites were produced at the Japan Atomic Energy Research Institute (currently Japan Atomic Energy Agency) and provided through PNNL. [7] Limited information of these materials is found elsewhere. [6]

Properties Evaluation

Dynamic elastic modulus was determined at room temperature using the impulse excitation of vibration method per ASTM Standard C1259-01.

Tensile properties of the composite materials were evaluated using specimens machined from flat plates so that the longitudinal direction was parallel to one of the fiber directions. Miniature tensile geometry that had been developed for neutron irradiation studies on ceramic composites was employed.[4] The rectangular geometry with the gauge size (length × width × thickness) of 12 mm × 4 mm × 2 mm is within a range where a systematic gauge size effect is observed. Tensile tests were conducted in accordance with the general guidelines of ASTM C1275-00. The tensile test incorporated several unloading/reloading sequences in order to allow analysis on the hysteretic response. For the testing at room temperature, the specimens were clamped by wedge grips with aluminum end tabs on both faces of the grip sections. The strain was determined by averaging the readings of strain gauges adhered to both faces of the center gauge section. The crosshead displacement rate was 0.5 mm/min for all tests.

Interlaminar shear strength (ILSS) of the composite materials was determined by a double-notched shear (DNS) test per ASTM C1292-00. The specimen dimensions were 20 mm x 4 mm x 2 mm so that two DNS specimens could be accommodated in a space for one tensile bar of 40 mm x 4 mm x 2 mm in the irradiation vehicle. The notch separation was chosen to be 6 mm. Trans-thickness tensile strength (TTS) of the composite materials was determined by a diametral compression test at room temperature. In this test, diametral compressive load applied to a small diameter disc (or truncated disc) specimen is converted to tensile load in the perpendicular orientation leading to the failure in trans-thickness tension. Details of the test procedure are given. [2] Microstructures and tensile fracture surfaces were examined with an optical microscopy and a field emission scanning electron microscopy (FE-SEM).

Results

Microstructures of the composites prepared on the polished cross-sectional surfaces are shown in Figs. 1-7. The micrographs reveal that all the CVI composite materials achieved reasonable intra-fiber-bundle matrix infiltration. However, it is noticed that some of the Hi-Nicalon™ Type-S composites do have substantial interlaminar pores compared to others. In the Hybrid CVI composite, micro-cracking within the CVI SiC matrix perpendicular to the graphite fiber axis direction is extensively observed.

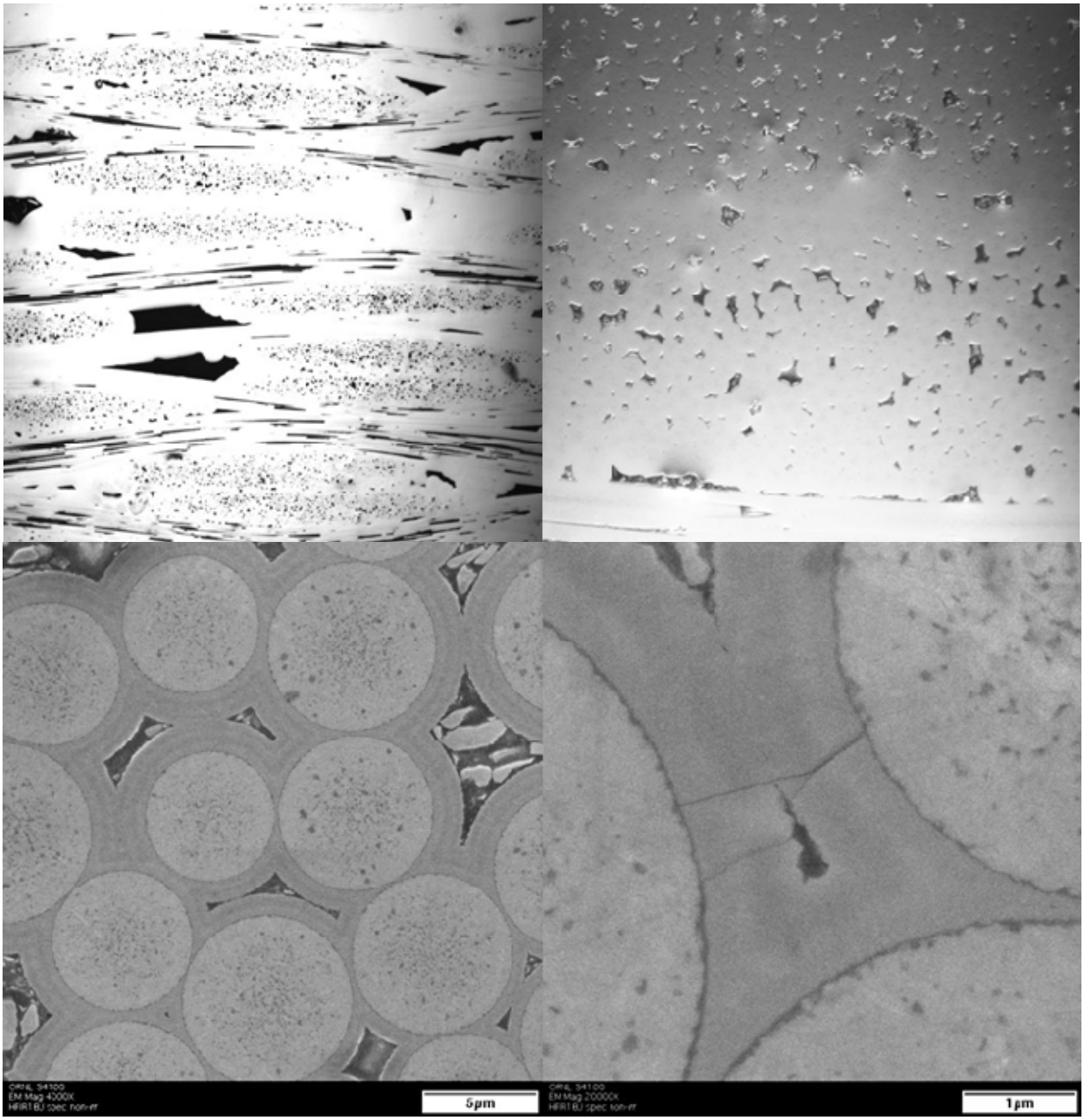

Figure 1. Cross sectional polished surface image of TySA-CVI-Ref composite.

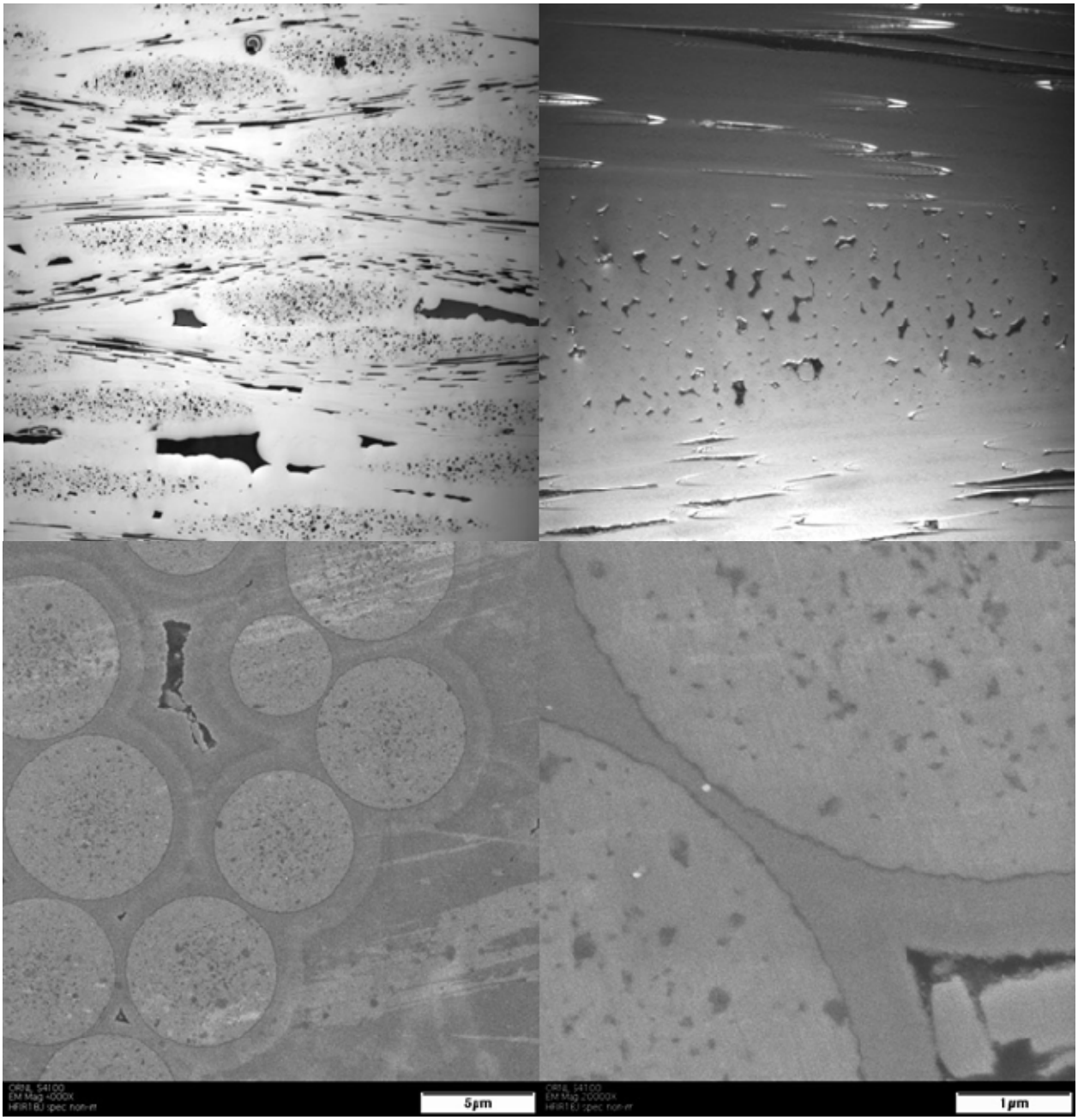

Figure 2. Cross sectional polished surface image of TySA-CVI-TI composite.

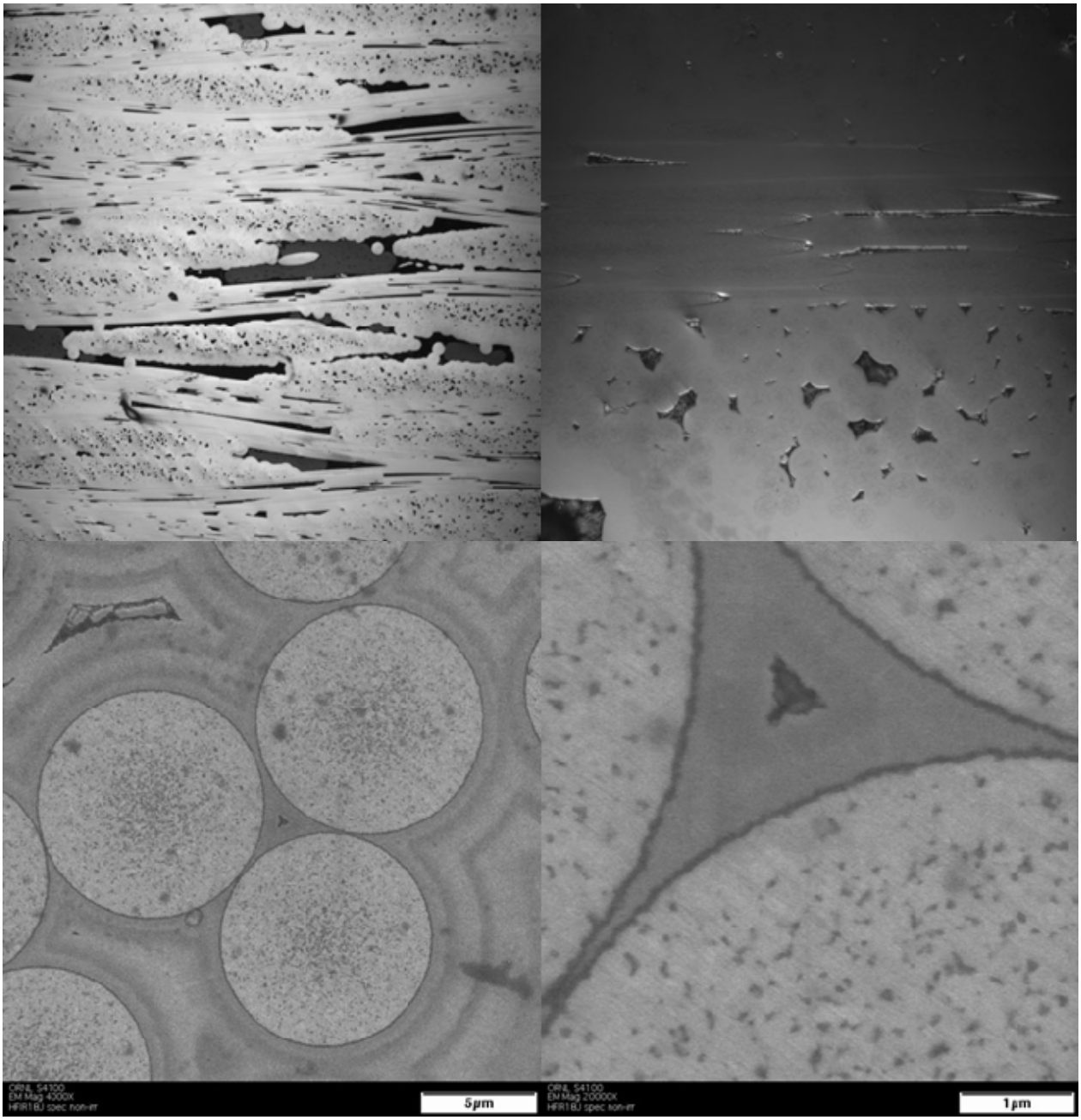

Figure 3. Cross sectional polished surface image of TySA-CVI-TF composite.

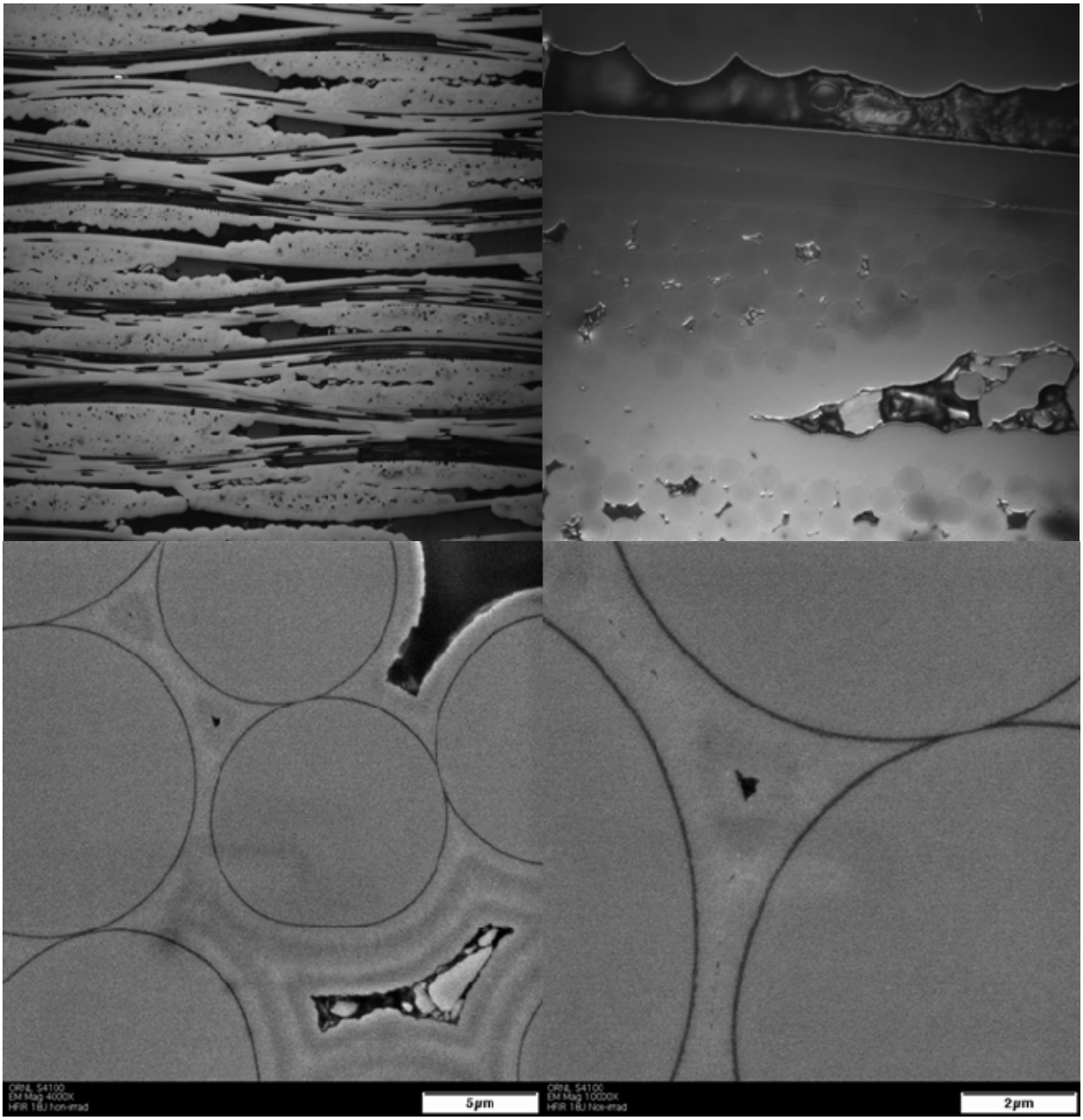

Figure 4. Cross sectional polished surface image of HNLS-CVI-Ref composite.

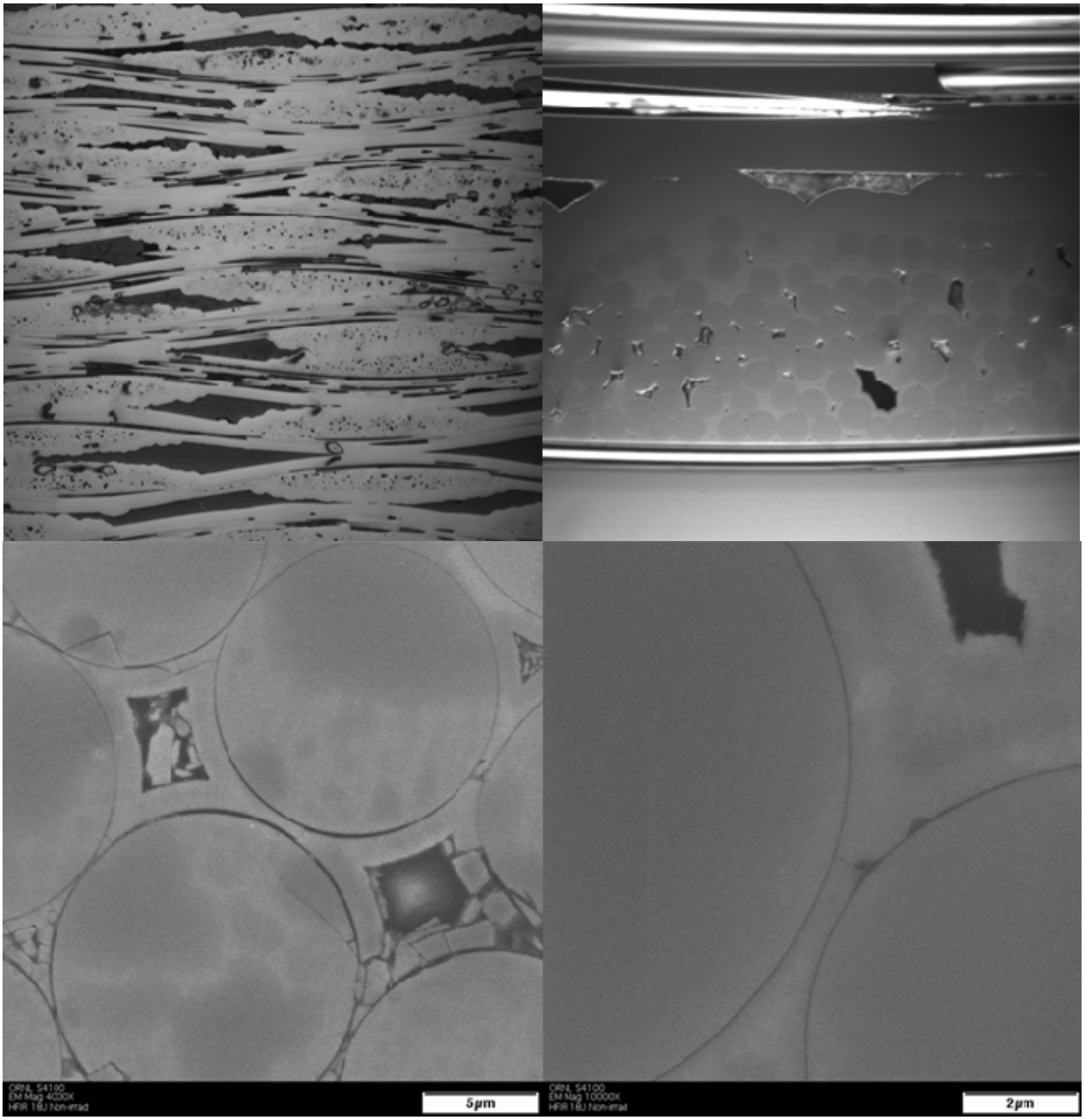

Figure 5. Cross sectional polished surface image of HNLS-CVI-TI composite.

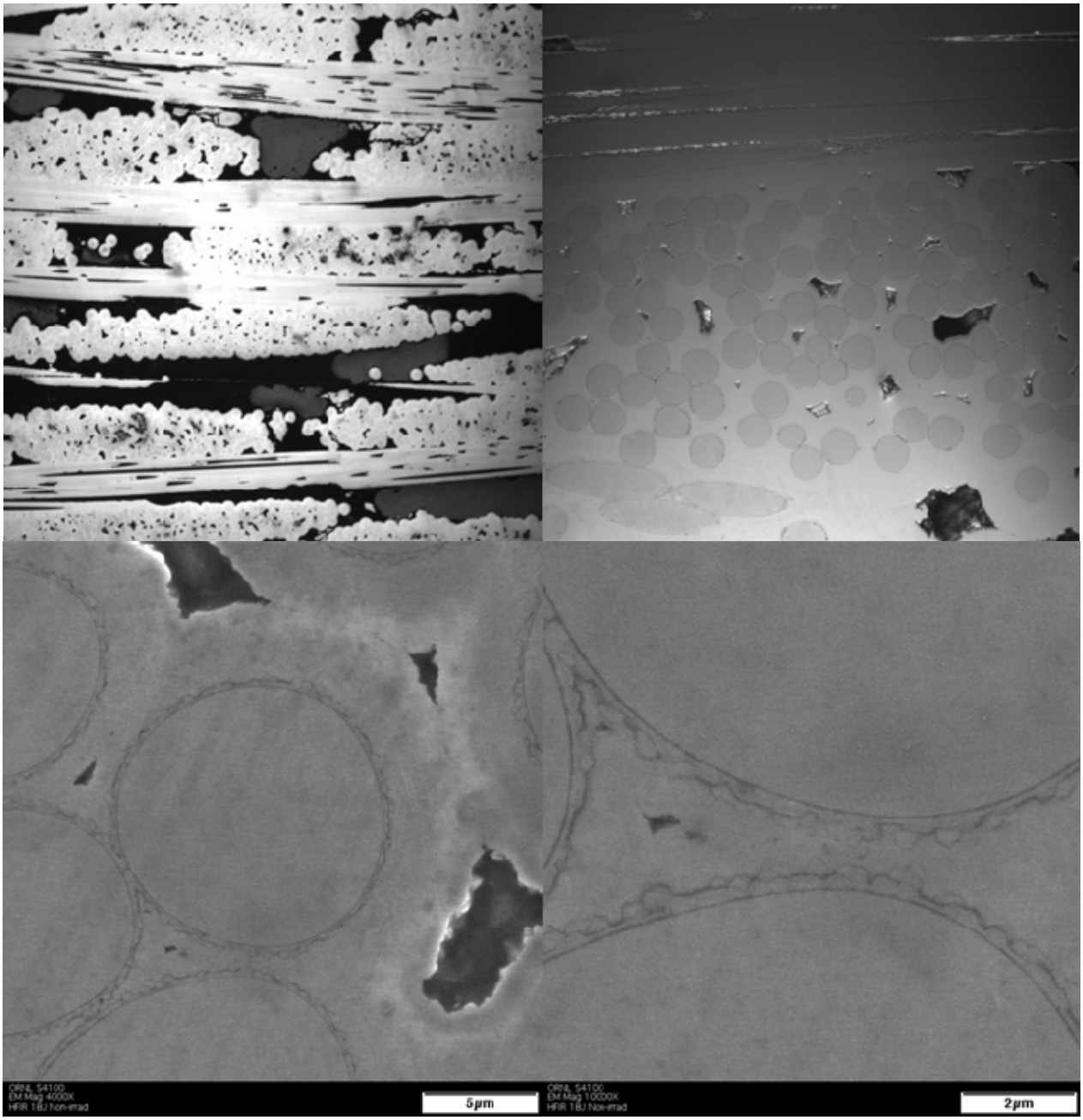

Figure 6. Cross sectional polished surface image of HNLS-CVI-ML composite.

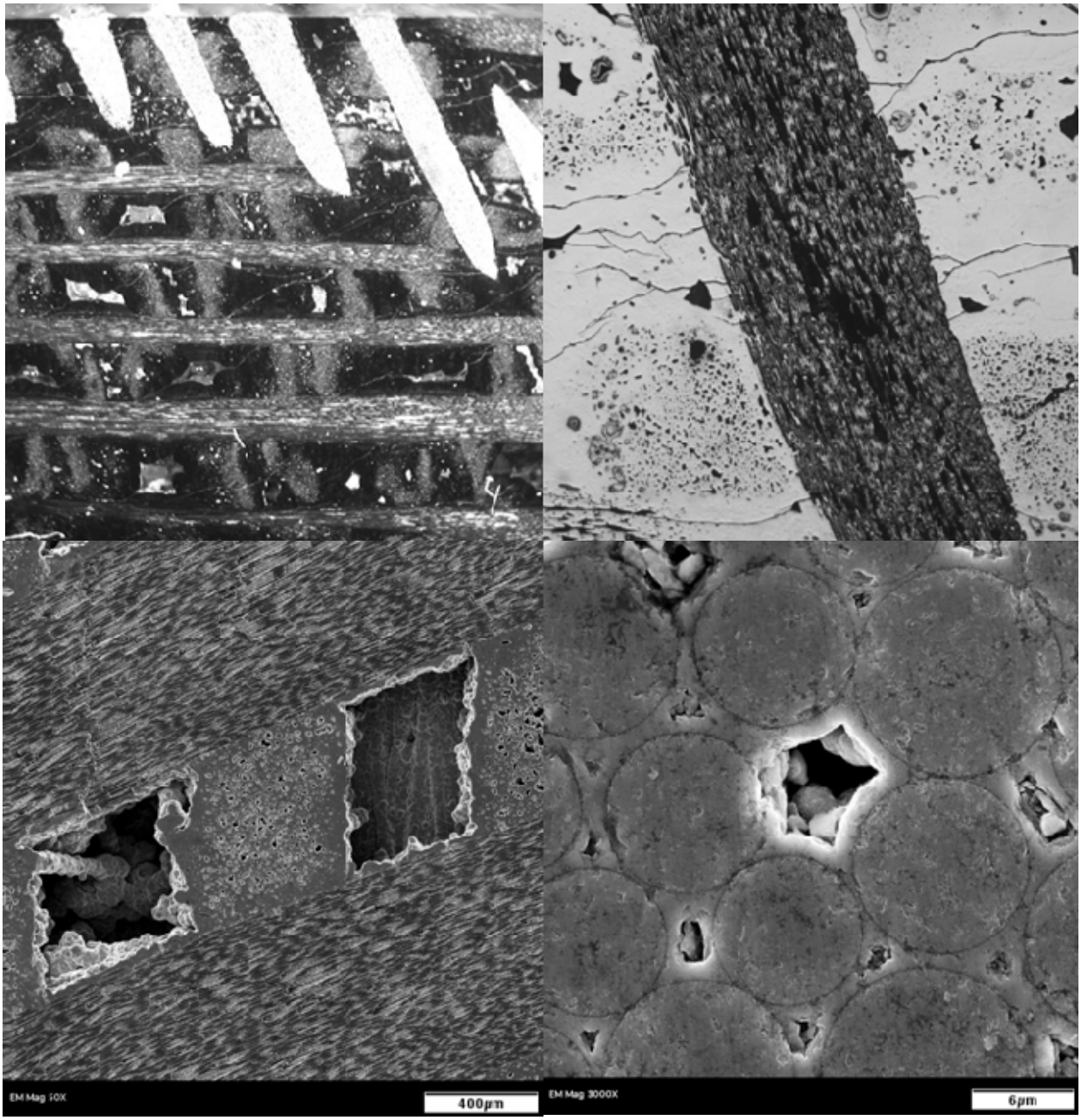

Figure 7. Cross sectional polished surface image of HNLS-CVI-ML composite.

Tensile stress-strain charts are presented in Fig. 8. The intermittent unloading-reloading sequences were incorporated for future evaluation of the interfacial sliding properties. The 2D CVI composites exhibited similar tensile behaviors regardless of fiber type or interphase. The initial tangent modulus, the proportional limit stress (PLS), and the ultimate tensile stress (UTS) for each 2D CVI composites appear to be typical for similar materials. The results from Hi-Nicalon™ Type-S reference and thin interphase 2D composites will be given in a future report. The Hybrid 3D composite exhibited low initial tangent modulus and poor tensile strength due likely to both the matrix pre-cracking and the small volume fraction of the SiC fibers in the loading direction. The NITE composite exhibited the significantly higher initial tangent modulus, PLS, and UTS compared to the CVI composites. The quantitative results are summarized in Table 2.

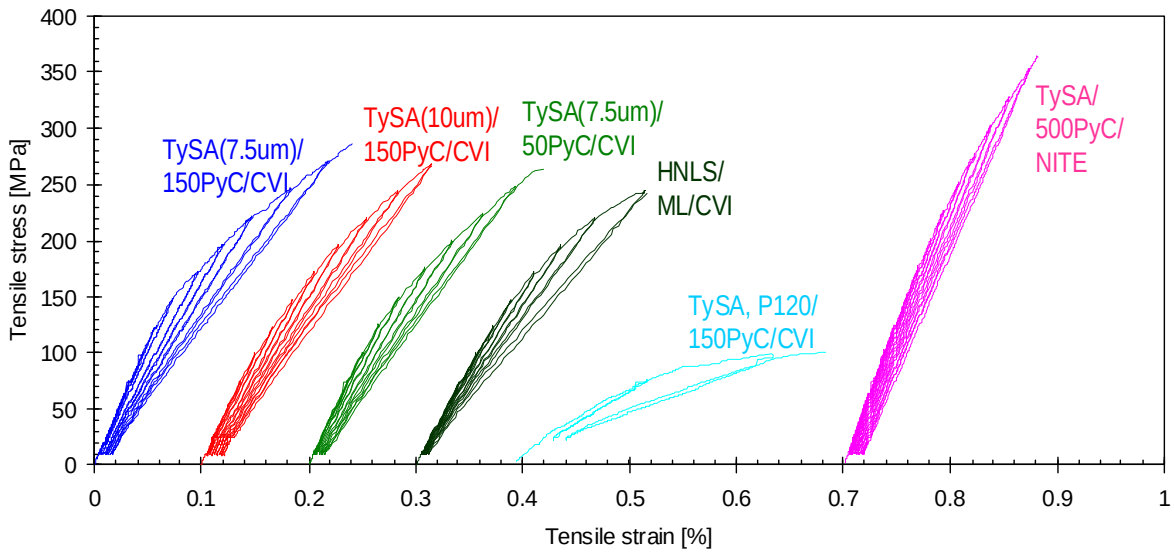

Figure 8. Tensile stress-strain behaviors of the composite materials at room temperature.

Table 2 – Summary of tensile properties of the composite materials. The numbers in parentheses represent one standard deviation.

Material	E [GPa]	PLS [MPa]	UTS [MPa]	Number of test
TySA-CVI-Ref	212 (12)	110 (24)	285 (26)	7
TySA-CVI-TF	201 (13)	104 (20)	304 (34)	3
TySA-CVI-TI	236 (49)	73 (25)	272 (10)	3
HNLS-CVI-TI	182 (8)	104 (16)	232 (27)	4
TySA-NITE	271 (9)	182 (55)	357 (8)	3
Hybrid-CVI	101 (38)	64 (41)	111 (71)	4
Hybrid-CVI tested with specimen dimensions 6 mm x 2.5 mm x 50 mm	95 (10)	82 (14)	98 (3)	n/a

Typical results of the interlaminar shear strength tests are given in Fig. 9. All the Tyranno™-SA3 2D composites exhibited similar values of shear strength at 30 to 35 MPa. The Hi-Nicalon™ Type-S multilayer composite showed slightly lower shear strength as anticipated from the slightly enhanced interlaminar porosity. The interlaminar shear strength of the PyC interphase Hi-Nicalon™ Type-S composites suffered very significantly from the apparently very poor interlaminar matrix densification. The Hybrid 3D composite exhibited the interlaminar shear strength of ~25 MPa, which is slightly lower than those for the Tyranno™-SA3 2D composites, in spite of the presence of the trans-thickness graphite fibers. The lower-than-anticipated shear strength of the Hybrid 3D composite may be attributed to the extensive matrix cracking introduced by the thermal expansion mismatch between the SiC matrix and the graphite fibers. The NITE composite exhibited the highest interlaminar shear strength owing to the dense SiC matrix.

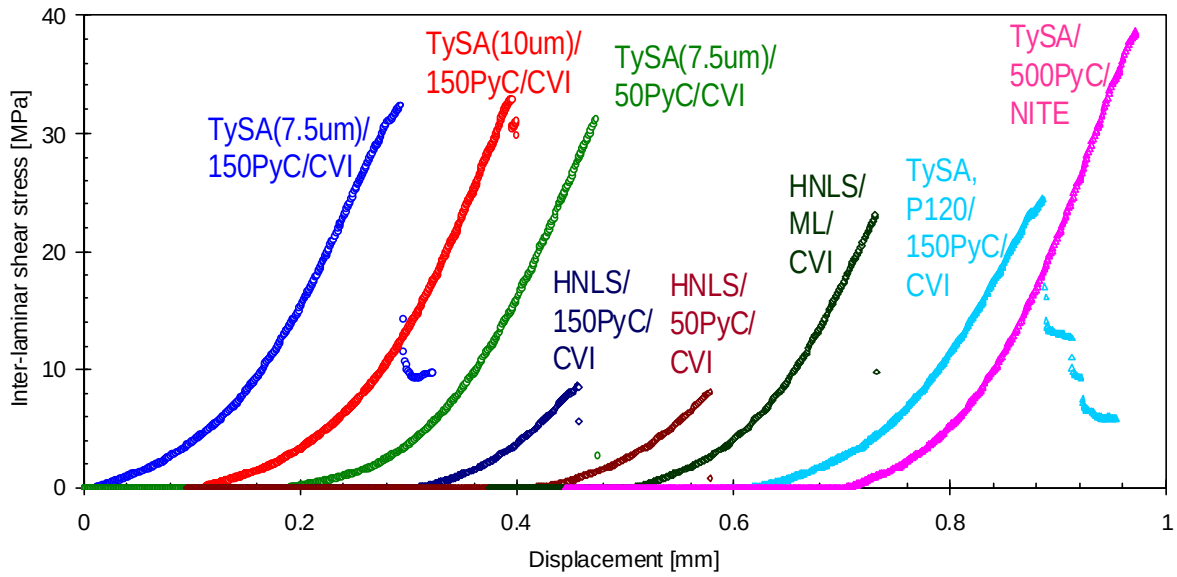

Fig. 9. Interlaminar shear stress vs. crosshead displacement in double notched shear testing of various SiC composites.

Table 3 – Summary of interlaminar shear strength of the composite materials. The numbers in parentheses represent one standard deviation.

Material	ILSS [MPa]	# of test
TySA-CVI-Ref	31.2 (3.7)	8
TySA-CVI-TF	31.9 (13.2)	8
TySA-CVI-TI	29.1 (5.8)	7
HNLS-CVI-Ref	10.8 (5.7)	8
HNLS-CVI-TI	9.6 (2.7)	4
HNLS-CVI-ML	23.3 (5.5)	8
Hybrid-CVI	24.8 (3.5)	6
TySA-NITE-LG	37.0 (3.7)	2

The trans-thickness tensile strength was evaluated for the Tyranno™-SA3 composites with CVI and NITE matrices. The result is given in Fig. 10 and Table 4. The tensile strength values appeared to be ~26 MPa for the CVI composite and ~32 MPa for the NITE composite. The result with CVI composite is consistent with the previous work, in which the trans-thickness tensile strength was measured to be 25 to 30 MPa for 7 different CVI composites with Tyranno™-SA3 or Hi-Nicalon™ Type-S reinforcements.[2] The higher strength for the NITE composite can be attributed to the higher density of the NITE matrix.

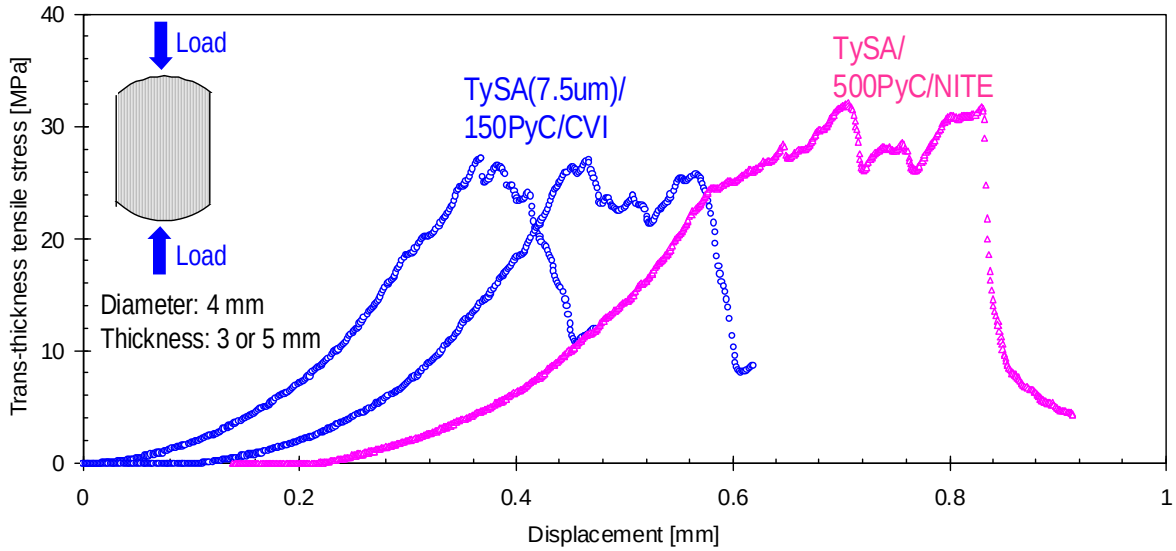

Fig. 9. Trans-thickness tensile stress vs. crosshead displacement in diametral compression testing of Tyranno™-SA3 CVI and NITE composites.

Table 4 – Summary of trans-thickness tensile strength of the composite materials. The numbers in parentheses represent one standard deviation.

Material	TTS [MPa]	Number of test
TySA-CVI-Ref	26.4 (1.4)	5
TySA-NITE-LG	32.0 (-)	1

The dynamic Young's modulus had been measured before the irradiation capsule was constructed for all the samples which had been supposed to be irradiated and of straight rectangular geometries with reasonable length to thickness ratios. Table 5 summarizes the result of the modulus measurement. The irradiated dynamic modulus will be measured as a part of the post-irradiation examination campaign and will be directly compared with the pre-irradiation values for individual specimens.

Table 5 – Summary of the Young's modulus of the SiC ceramics and composites. The numbers in parentheses represent one standard deviation.

Material	Dynamic Young's modulus [GPa]	Number of test
R&H CVD SiC	449 (1.2)	8
NITE Matrix SiC	347 (9.5)	5
TySA-CVI-Ref	254 (11.5)	50
TySA-CVI-TI	273 (11.9)	24
TySA-CVI-TF	250 (16.1)	24
HNLS-CVI-ML	210 (18.3)	24
Hybrid-CVI	129 (21.3)	20
TySA-NITE	335 (10.8)	22
HNLS-CVI-Ref	224 (11.0)	24
HNLS-CVI-TI	211 (36.6)	24
TySA-NITE-LG	370 (28.8)	31

In summary, the SiC-based composite specimens prepared for the irradiation study in the HFIR-18 experiment performed as expected in terms of axial tensile, interlaminar shear, and trans-thickness tensile properties, with the exceptions of interlaminar properties of the PyC-interphase Hi-Nicalon™ Type-S, CVI composites which appeared to have achieved poor interlaminar matrix densification. More detailed evaluation of unirradiated materials including thermal conductivity and fracture resistance is planned.

References

[1] T. Hinoki, N. Eiza, S.J. Son, K. Shimoda, J.K. Lee, and A. Kohyama, Ceramic Engineering and Science Proceedings 26 (2005) 399-405.
[2] T. Hinoki, Y. Maki, A. Kohyama, E. Lara-Curzio, and L.L. Snead, Ceramic Engineering and Science Proceedings 25 (2004) 65-70.
[3] A. Kohyama, 31st International Conference on Advanced Ceramics and Composites, Daytona Beach, 2007.
[4] T. Nozawa, Y. Katoh, A. Kohyama, and E. Lara-Curzio, in: R.H. Jones, A. Kohyama, and B. Riccardi, (Eds.), Fifth International Energy Agency Workshop on SiC/SiC Ceramic Composites for Fusion Energy Application, PNNL-SA-37623, Pacific Northwest National Laboratory, 2002, pp. 74-86.
[5] T. Nozawa, Y. Katoh, L.L. Snead, T. Hinoki, and A. Kohyama, Ceramic Engineering and Science Proceedings 26 (2005) 311-318.
[6] T. Nozawa, K. Ozawa, Y. Katoh, and A. Kohyama, Materials Transactions 45 (2004) 307-310.
[7] R. Yamada, N. Igawa, and T. Taguchi, Journal of Nuclear Materials 329-333 (2004) 554-557.